RESEARCH ARTICLE | NOVEMBER 28 2022

# Interpreting acoustic emissions to determine the weld depth during laser beam welding

Special Collection: Proceedings of the International Congress of Applications of Lasers & Electro-Optics (ICALEO 2022)

Lazar Tomcic ; Armin Ederer ; Sophie Grabmann ; Michael Kick ; Johannes Kriegler ;
Michael F. Zaeh

Check for updates

View Online    Export Citation

---

### Articles You May Be Interested In

A decision support system based on support vector machine for employee recruitment

*AIP Conference Proceedings* (November 2022)

Acoustic process monitoring during the laser beam welding of stainless-steel foils using an adjustable ring mode laser beam source

*J. Laser Appl.* (October 2024)

Inline failure detection in laser beam welding of battery cells: Acoustic and spectral emission analysis for quality monitoring

*J. Laser Appl.* (March 2024)

# Interpreting acoustic emissions to determine the weld depth during laser beam welding

View Online    Export Citation    CrossMark

Lazar Tomcic, [ID] Armin Ederer, [ID] Sophie Grabmann, [ID] Michael Kick, [ID] Johannes Kriegler, [ID] and Michael F. Zaeh

**AFFILIATIONS**

Technical University of Munich, TUM School of Engineering and Design, Institute for Machine Tools and Industrial Management (*iwb*), Boltzmannstrasse 15, 85748 Garching, Germany

## ABSTRACT

The interpretation of sensor system data is critical for monitoring industrial welding processes and providing reliable information about the condition of the weld seam. Previous investigations have shown that acoustic emissions of frequencies up to several kilohertz during laser beam welding are parameter-dependent and contain valuable information about the process. A microphone was employed to record the acoustic emissions produced when performing deep penetration laser beam welding of copper. Experiments were conducted in which the laser power and the feed rate were varied so as to obtain acoustic data comprising frequencies of up to 1 MHz. The signals were preprocessed and features were extracted using Fourier and wavelet analysis as well as speech analysis techniques. The relationship between the features extracted from the acoustic signal and the weld depth was modeled using Gaussian process regression. The results showed that acoustic emissions during laser beam welding can be used to predict the weld depth without having to rely on process parameters, i.e., the laser power and the feed rate. Overall, 17 features were extracted from acoustic signals, with the zero-crossing rate displaying the highest significance for determining the weld depth. These investigations open up new possibilities of robust quality assurance for laser beam welding applications based on acoustic emissions.

Key words: process monitoring, acoustics, laser beam welding, weld depth, green laser beam, machine learning, quality assurance

## I. INTRODUCTION

Quality assurance of joining processes on the basis of acoustic emissions has been the subject of research for many years. Numerous quality criteria have to be determined, which vary according to the type of joining technology used. In the case of laser beam welding, the weld depth is a relevant quality feature when it comes to determining the mechanical and electrical properties of the weld seam. However, it is difficult to measure due to short process times and the small processing zone involved. This paper describes the use of an acoustic sensor and machine learning methods to determine the weld depth in continuous-wave laser beam welding.

## II. STATE OF THE ART

Early investigations of acoustic emissions produced during laser beam welding found that the dominant frequency range of

the signal depends on the process regime.[1] In the case of deep penetration welding, the vapor plume expanding at high pressure from the keyhole[2] and the fluctuating vapor flow rate lead to variations in the acoustic signal.[3] Studies with sensors covering frequencies of up to 1 MHz were able to measure ultrasonic acoustic emissions near the process zone during laser beam welding.[4] A threshold-based statistical method of analyzing the frequency patterns of the acoustic emissions was considered for determining the condition of the weld seam using conventional microphones.[5] However, one difficulty of this method is that it might lack reproducibility when the position of the sensor is changed, since the emission spectra do not necessarily show the same distribution pattern. A different approach was taken by Huang *et al.*[6] who identified the relevance of the power spectral density when distinguishing between full and partial penetration welding. However, the threshold-based noise reduction techniques employed can lead to challenges regarding

reproducibility when applied in a different experimental environment. Schmidt et al.[7] used a convolutional neural network for analyzing the autocorrelation of the acoustic signal to determine the feed rate and achieved classification accuracies of above 80%. Wasmer et al.[8] used wavelet packet decomposition to extract features from the time-frequency domain by choosing relevant relative energies. The authors achieved an accuracy of 74% using discrete wavelet transformation (DWT), which enabled them to classify the process into four predefined categories related to the process regime and the occurrence of spatter. Adopting this approach and using a graph support vector machine, a classification accuracy of 85.9% was achieved.[9] Yusof et al.[10] demonstrated the use of airborne acoustic signals for monitoring pulsed laser beam welding processes.

Recent investigations focused on retrieving information on the weld depth of laser beam welded joints from the acoustic signature. A deep learning approach based on a feed-forward neural network was employed by Huang et al.[11] Although the model showed promising results, it involved 28 observations (i.e., weld seams), and the train-test split was 50/50. This might lead to bias and overfitting due to the complexity of the regression task. Following an extensive feature engineering process, Yusof et al.[12] identified relevant features that lead to a mean prediction error of only 4.08%. Aside from laser power and pulse duration, other parameters, such as the feed rate, remained constant in all experiments. When using the same sensor as the one presented in this study, Authier et al.[13] found a relationship between acoustic emissions within the frequency range of 40–90 kHz and the weld depth for pulsed laser beam welding. However, no approach for predicting the weld depth based on findings was developed.

## III. OBJECTIVE AND APPROACH

Examining acoustic emissions during laser beam welding has been shown to be a feasible method for the purpose of quality assurance. This study aims to expand on previous findings with an emphasis on

- identifying relevant acoustic features with the discriminatory ability to
- substitute process parameters, i.e., the laser power and the feed rate, as model inputs and to
- use a Gaussian process regression (GPR) for the modeling process to predict the weld depth of laser beam weld seams.

## IV. EXPERIMENTAL SETUP

A state-of-the-art laser beam source (TRUMPF TruDisk 1020) with a maximum power output of 1000 W and emission at 515 nm was used in these investigations. Combined with the scanner optics (TRUMPF PFO 20-2), a focal diameter of 150 μm was achieved on the workpiece. Bead-on-plate weld seams were made on oxygenfree copper plates with a thickness of 1 mm. Figure 1 shows the positioning of the laser-based acoustic sensor (Xarion Eta250). A description of the sensor principle can be found in Ref. 14. Studies showed that the absorptivity of acoustic waves in air increases with frequency.[15]

Therefore, the sensor was positioned at a distance of 20 mm from the process zone to obtain a broad frequency range of up to
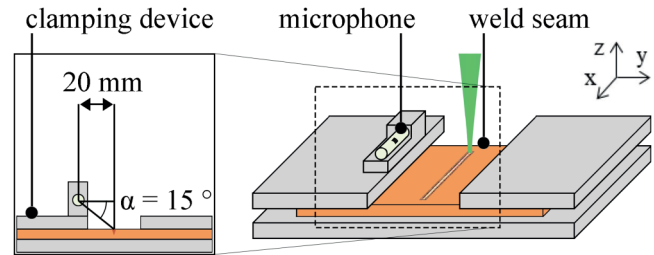


**FIG. 1.** Experimental setup for investigations showing the sensor position.

1 MHz using a sampling rate of 3.125 MHz. All data processing was performed with RStudio (stable release 2022.02.2 + 485) on a computer fitted with an Intel Core i7-4770 CPU, a Nvidia GeForce GTX 1660 graphics card, and 16 GB of RAM. Variation of the laser power $P$ and feed rate $v$ resulted in a total of 87 specimens, each with a weld seam length of 10 mm. See Table III in the Appendix for the design of the experiment.

## IV. DATA PREPROCESSING

The optical microphone was triggered manually and the acoustic emission recordings were trimmed such that they only contained the time segment of the welding process. This involved applying the amplitude envelope function based on the Hilbert transform provided by R package *seewave*.[16] This resulted in a mean deviation between detected and expected signal durations of 0.2 ms or 648 samples. The duration of the trimmed process signals depended on the feed rate and was between 26.3 and 100.0 ms or 83 150 and 313 310 samples.

## V. FEATURE ENGINEERING

When extracting features from a signal, the goal is to reduce dimensionality and obtain relevant data concerning the target variable. To reduce the possibility of overfitting during the modeling phase,[17] high intercorrelations and collinearities between the features should be avoided. In the case of acoustic signals, information can be extracted from the time, frequency, and time-frequency domain. A total of 17 features were extracted from the recorded acoustic emission of each experiment during the feature engineering process.

In the time domain, mean, median, standard deviation (SD), and mean absolute deviation (MAD) were extracted. Skewness and kurtosis were also calculated, as they characterize the appearance of the amplitude distribution.

Features from other application areas, such as speech and voice processing, were also obtained from the raw signal. The zero-crossing rate (ZCR) is the rate of a signal's sign changes[18] and is defined as:

$$ZCR = \frac{1}{N-1} \sum_{n=1}^{N-1} |sgn[x_i(n)] - sgn[x_i(n-1)]|, \quad (1)$$

where $N$ is the length of the signal $x_i$ and $sgn$ is the sign function

according to

$$sgn[x_i(n)] = \begin{cases} 1, & x_i(n) \geq 0 \\ -1, & x_i(n) < 0 \end{cases}. \tag{2}$$

The ZCR showed a positive correlation with the feed rate and a good discriminatory capability for signals with identical feed rates and different laser powers, as shown in Fig. 2.

Short-time energy (STE) is defined as average energy per segment of a signal[18] and is often used to detect environmental sound:

$$STE = \frac{1}{N} \sum_{n=1}^{N} |x_i(n)|^2. \tag{3}$$

The STE feature was applied to 10 ms segments with a 50% overlap using the rectangular window function. The median (STE_Median), mean absolute deviation (STE_MAD), and standard deviation (STE_SD) were calculated. Additional features were selected in the frequency domain from previous studies that contributed to correct classification or regression. The band power BP (Ref. 6) was extracted according to

$$BP = \sum_{f_j}^{f_k} PSD_{x_i}. \tag{4}$$

Here, $f_j - f_k$ is the frequency range over which the power spectrum density (PSD) of the signal $x_i$ is integrated. According to Huang et al.,[19] the acoustic emissions during laser beam welding of fully and partially penetrated welds differ significantly in the frequency range of 0.5–1.5 kHz. Similar results were reported for the frequency ranges of 7–10[1] and 40–90 kHz.[13] The band power was calculated using a Hann window function for three frequency ranges, resulting in three distinct features. Ever since the introduction of wavelet transformation in 1990,[20] the method has been used increasingly in a number of applications for the purpose of
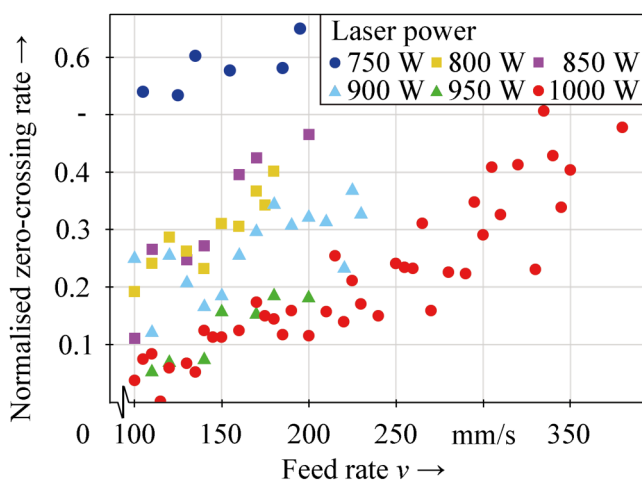
time-series analysis.[21] In the present study, continuous wavelet transformation (CWT) was performed using the Morlet wavelet. CWT was chosen in favor of DWT due to its insensitivity to noise and its higher resolution. The continuous wavelet transformation of a time series is defined as

$$W_n(s) = \sum_{n'=0}^{N-1} x_{n'} \psi^* \left( \frac{(n' - n)\delta t}{s} \right). \tag{5}$$

Here, $\delta t$ represents the time increment and $s$ represents the scale factor of the wavelet function $\psi_0$.[21] The Morlet wavelet function is defined as

$$\psi_0(\eta) = \pi^{-1/4} e^{i\omega_0 \eta} e^{-\eta^2/2}, \tag{6}$$

where $\omega_0$ is the nondimensional frequency and $\eta$ is the nondimensional time parameter.[21] Compared to the short-time Fourier transformation, the advantages of this method are that it is less sensitive to noise, it retains the time information, and it can be used with nonstationary signals. The recorded signals were downsampled to 300 kHz to reduce the necessary computation time for obtaining the CWT. The transformation is applied to discrete time series with the time increment $\delta t$ and the scale factor $s$, i.e., the position on the time axis and the stretching of the wavelet. The result is a coefficient matrix of the form $M \times N$, where $M$ represents the scales and $N$ represents the samples. The wavelet at scale $s$ is conjugated with the signal at shift $n$, yielding a value close to 1 for high congruence and close to zero for none. The negative values and complex numbers were not considered in this work.

In order to distinguish the acoustic signals for different laser powers, the wavelet scale distributions of acoustic signals from welding processes with the same feed rate but at different laser powers were compared using the following steps:

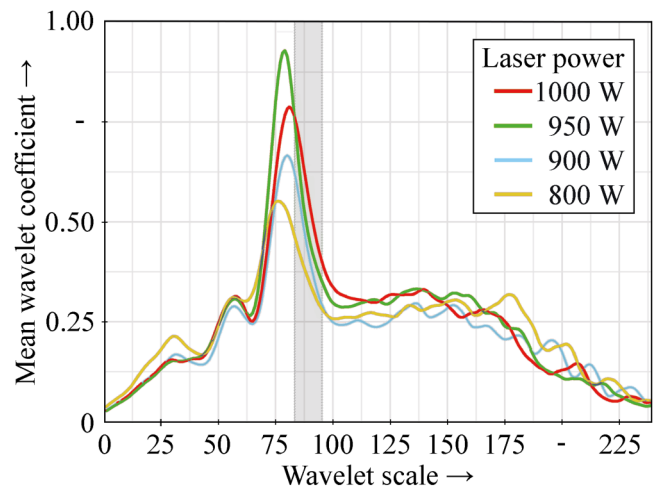**FIG. 2.** Normalized zero-crossing rate over feed rate.

**FIG. 3.** Normalized mean wavelet coefficient over a wavelet scale for acoustic signals obtained with four laser powers at a constant feed rate of $v = 110$ mm/s; the gray area indicates the wavelet scales 84–88.
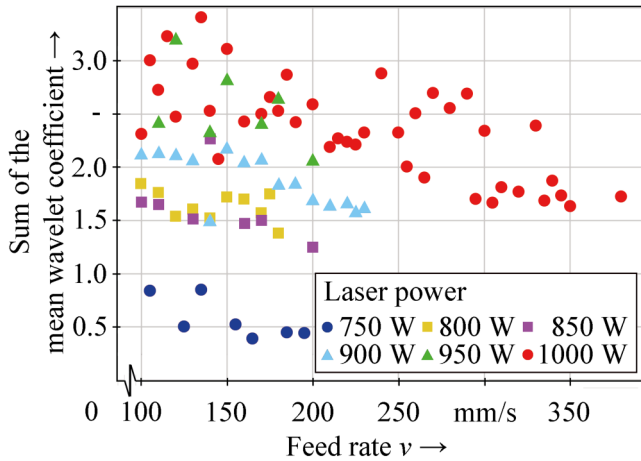
**FIG. 4.** Sum of mean wavelet coefficients for scales 84–88 over the feed rate.

- create datasets with identical feed rates but different laser powers;
- calculate the mean value for each wavelet scale;
- compare the individual wavelet scales for each signal using the condition $P1 > \ldots > P1 + n$, where $P1$ is the highest laser power in the test sets; and
- return the wavelet scales where the condition is true.

The wavelet scales 84–88 were identified as good discriminators for the dataset. Interestingly, they are equivalent to a frequency range of ~7–10 kHz. Figure 3 presents an example of acoustic signals with four different laser powers at an identical feed rate, with the governing wavelet scales marked in gray.

Totaling the wavelet coefficients for each scale was found to be a successful approach for datasets with constant feed rates.[10] Applying the same method for this study would have led to a high degree of correlation with the duration of the signal. A long signal caused by a low feed rate results in a higher sum of wavelet coefficients, which can be misleading when the data consist of experiments with different feed rates. This may reduce the feature's informative value for the model. Therefore, the mean values of the selected wavelet scale coefficients were accumulated and chosen as a feature (CWT_Scale) for further modeling. The results are shown in Fig. 4 for each experiment.

Thanks to the high accuracy of manual trimming, the signal duration in milliseconds could be chosen as an additional feature.

## VI. WELD DEPTH PREDICTION

GPR was employed to determine the weld depth based on the features extracted. A Gaussian process is a finite number of random variables with a joint Gaussian distribution[22] and is specified by

$$f(x) \sim GP(m(x), \ k(x, x')). \tag{7}$$

Here, $m(x)$ is the mean function and $k(x, x')$ is the covariance function.[22] The joint distribution of the training data $f$ and the test data

$f_*$ can be expressed as

$$\begin{bmatrix} f \\ f_* \end{bmatrix} \sim N\left( \begin{bmatrix} \mu \\ \mu_* \end{bmatrix}, \begin{bmatrix} k & k_* \\ k_*^T & k_{**} \end{bmatrix} \right). \tag{8}$$

Here, $\mu$ is the mean of the training data and $\mu_*$ is the mean of the test data. The variable $k$ indicates the covariance of the training data, $k_*$ indicates the covariance between training and test data, and $k_{**}$ indicates the covariance of the test data.[22]

In order to predict the test data, the equation is arranged to retrieve the conditional distribution $f_*$ for a given $f$:

$$f_* | f \sim N(\mu_* + k_*^T k^{-1} (f - \mu), \ k_{**} - k_*^T k^{-1} k_*). \tag{9}$$

Equation (9) can be used for nonlinear regression tasks. In this paper, three covariance functions[23] were applied:

- the radial basis function (RBF),

$$k(x, x') = \exp(-\sigma |x \cdot x'|^2), \tag{10}$$

- the linear function (LF),

$$k(x, x') = x \cdot x', \quad \text{and} \tag{11}$$

- the polynomial function (PF),

$$k(x, x') = (\sigma \cdot x \cdot x')^p. \tag{12}$$

Here, $\sigma$ and $p$ are the hyperparameters that have to be set. A detailed explanation of GPR and the covariance functions can be found in Ref. 22. Due to the high feed rate in combination with the short weld seam length that was applied for all experiments, the acoustic signals were assumed to be stationary, and the weld depths were assumed to be constant. Figure 5 shows the weld depths measured from metallographic cross sections.
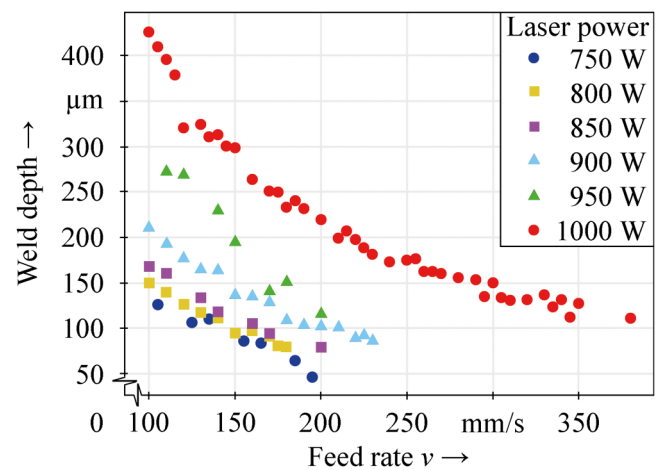


**FIG. 5.** Measured weld depth over feed rate for experiments performed.

Univariate filter methods were applied before modeling, in which the relevance of features (predictors) and the target variable were evaluated based on correlations, as shown in Fig. 6. According to Guyon et al.,[17] this method can help identify feature pairs that show a perfect correlation with each other and, thus, can be assumed redundant. One of the features should subsequently be removed before the modeling process. In the case of the SD and the root mean square (RMS) of the acoustic signal, a perfect positive correlation value of 1.0 was observed. Therefore, the latter was excluded as a feature. All other features had values below 1.0 and above −1.0. Features that showed a low correlation with the target variable, i.e., the weld depth, were not excluded as this method does not account for feature dependencies. Thus, a wrapper-based approach was employed.

Nested k-fold crossvalidation was selected as a resampling method. Hyperparameters were tuned in the inner-most loop. A feature selection method was applied in the middle one, and the outer loop was considered for model validation. The resampling method is described by Vabalas et al.[24] in detail. The data in each loop were divided into five different folds with a random train-test split of 80/20 for each loop. The R package *Kernlab* was used for the modeling process.[23] The hyperparameter tuning was performed automatically. In order to identify the best feature subset for each covariance function, recursive feature elimination (RFE) was performed as part of the modeling process.[25] Features were ranked by importance (excluding the lowest-ranked feature in each iteration), with the predictors forming the inputs and the model performance measured by the RMSE as the output. When the lowest feature count, i.e., one, was reached, the feature subset with the best model performance was selected. According to Vabalas et al.,[24] this method is suitable for tasks with small observation sizes and leads to model
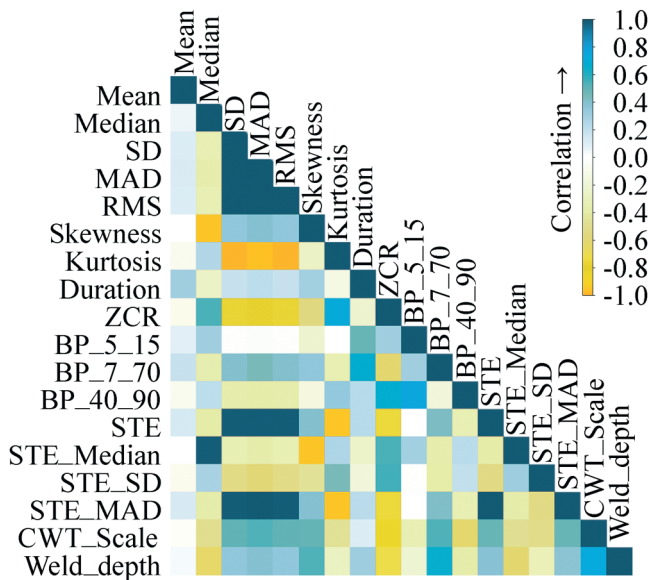
results having a low bias. The highest accuracy was achieved with GPR-LF, though it should be noted that GPR-PF achieved comparable results with only two features. Although all models required a computation time of less than 1.5 min, differences by a factor of more than four were observed, as shown in Table I.

A feature-to-observations ratio of below 1:2 is less likely to overfit.[24] Thus, the number of features selected by the wrapper method is in good accordance with these results. Table II displays a ranking of the relevant features revealing the same top eight features for GPR-RBF and GPR-LF models. The STE was ranked third, although the correlation with the weld depth was not significant as depicted in Fig. 6. For the GPR-PF model, only ZCR and STE_MAD were selected by the RFE. The features Mean, Duration, BP_5_15, and STE_SD were not part of the feature subset with the best model performance for any of the covariance functions.

A comparison of the mean predicted weld depth from the GPR models with the true weld depth is shown in Fig. 7. The bars indicate 95% confidence intervals for five training repetitions.

The Pearson correlation coefficient (PCC) provides a covariance measurement for all predictions. For a better visualization of confidence intervals, only predictions with a true weld depth of 100–350 $\mu$m and a point distance of 25 $\mu$m were used to generate Fig. 7. The predicted weld depths tend to be underestimated at high values, which is indicated by a shift in data points to the right-hand side of the dotted line. The best PCC was achieved with the GPR-RBF model. Relevant features can be extracted in all domains. The laser beam deep penetration welding process is characterized by the formation of a keyhole within the melt pool. The keyhole is held open by the balance of surface tension, ablation pressure, and excess pressure.[26] Klein et al.[27] found that the melt pool oscillates in radial, axial, and azimuthal modes at frequencies that are determined by physical and thermal constants of the material. The investigations of Gu et al.[28] concluded that the oscillation could lead to a sudden change in keyhole geometry, altering the coupling between the laser beam and the liquid material and eventually causing a fluctuation of the excess pressure. The acoustic emission during laser beam deep penetration welding corresponds to fluctuation in excess pressure.[29] Ao et al.[30] showed that for laser beam deep penetration welding, an increase in feed rate for a constant laser power leads to an increase in the amplitude of the acoustic emission and a positive shift of the dominant frequencies of the signal. The ZCR is a measure for the frequency content of a signal, thus the good discriminatory ability for different machine parameters and the high feature rank. This feature is often selected to classify music genres but also as a technique to estimate the fundamental frequency of a signal and is, hence, often used as a discriminator.[31] In speech recognition, ZCR is used as a feature for detecting fricatives, a term from linguistics referring to sounds

**FIG. 6.** Correlation matrix for features extracted and weld depth.

**TABLE I.** Results of the weld depth prediction for three different GPR models.

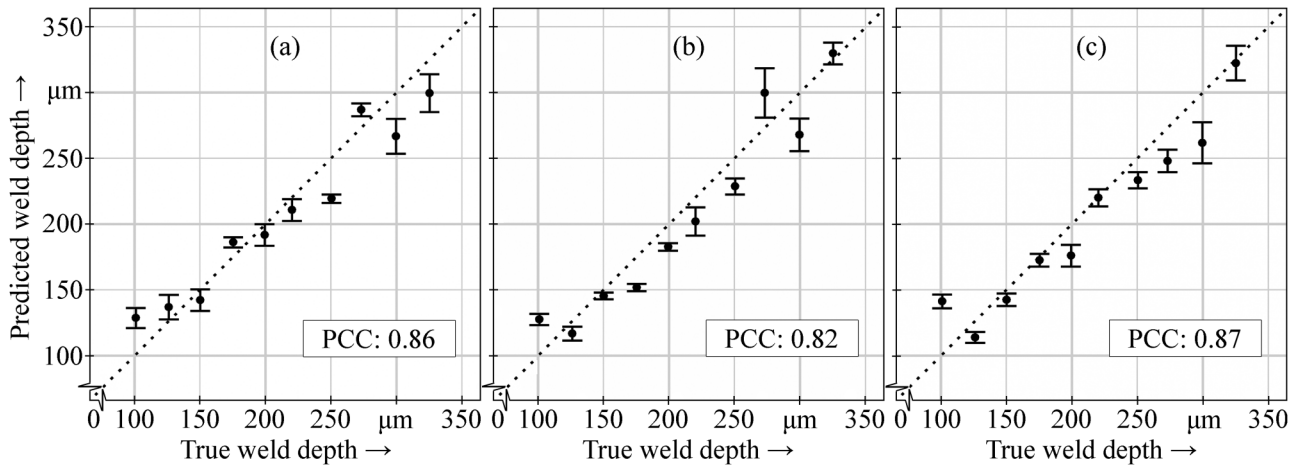|  | GPR-LF | GPR-PF | GPR-RBF |
| --- | --- | --- | --- |
| RMSE ($\mu$m) | 42.5 | 43.8 | 48.4 |
| No. of features | 12 | 2 | 11 |
| Computation time (s) | 26 | 89 | 19 |

**FIG. 7.** True weld depth over predicted weld depths for (a) GPR-LF, (b) GPR-PF, and (c) GPR-RBF.

produced by friction from outflowing air, for instance moving over the lips and teeth.[32]

The vapor plume expansion out of the keyhole during deep penetration welding is perceived as a loud hissing sound by the human auditory system, which corresponds to a fricative sound. Features relating to short-time energy were also considered important, especially the STE_MAD, which is in good accordance with the classification results of Yusof et al.[10] The adapted feature CWT_Scale[10] also proved to be relevant and is equivalent to the relevant frequency range of ~7–10 kHz reported by Mao et al.[1] In contrast, the ZCR contains the whole frequency range of the signal and not a specific spectrum, which makes it more sensitive to frequency shifts. It is assumed that this is one of the reasons why the CWT_Scale feature was ranked less significant for final models. Although Authier et al.[13] used the same sensor as described in this investigation, the reported band power between 40 and 90 kHz was not considered relevant for two out of three models. This might be because the feed rate in the work described here was not constant

for all experiments. Like CWT_Scale, the band power features focus on a narrow frequency spectrum and are less sensitive to frequency shifts caused by a variation of the feed rate. In addition, unlike Huang et al.,[19] no noise reduction techniques were used, which may also have a negative impact on the significance of these features for the modeling process. Even though the mean value was not selected in all models, the median and dispersion measures (SD, MAD) proved to be relevant for GPR-LF and GPR-RBF. The duration was not an important feature although it implicitly contains information about the feed rate.

## VII. CONCLUSION AND OUTLOOK

In this work, the weld depth of laser beam welded joints was determined on the basis of acoustic emissions using Gaussian process regression. A total of 17 acoustic features were preselected based on existing studies and the state-of-the-art audio analysis. These features were subsequently extracted from the acoustic signals produced by various welding processes. In addition, a modified wavelet coefficient was selected as a feature by identifying wavelet scales that are suitable to discriminate between laser powers at identical feed rates. Recursive feature elimination was performed prior to modelling, resulting in different feature subsets for each selected model. While the regression model with the linear covariance function performed best in terms of RMSE, the radial basis function achieved the highest PCC. For the polynomial function, only the zero-crossing rate and the mean absolute deviation of the short-time energy were selected as features. Both features were ranked as important for all models, which underlines their informative value for the target variable. The findings of this work represent a method of robust quality assurance in laser beam welding, which is based on acoustic emissions and does not require process parameters, i.e., the laser power and feed rate, as model inputs. Further research will elaborate on this approach to identify additional features. For the features related to short-time energy, other parameters, e.g., window functions and overlap percentage, should be investigated to potentially increase the quality of these features with regard to predicting the weld depth.

**TABLE II.** Ranking of selected features after RFE for each covariance function.

| Rank | GPR-LF | GPR-PF | GPR-RBF |
|---|---|---|---|
| 1 | ZCR | ZCR | ZCR |
| 2 | STE_MAD | STE_MAD | STE_MAD |
| 3 | STE | — | STE |
| 4 | CWT_Scale | — | CWT_Scale |
| 5 | Median | — | Median |
| 6 | MAD | — | MAD |
| 7 | SD | — | SD |
| 8 | STE_Median | — | STE_Median |
| 9 | Kurtosis | — | BP_7_10 |
| 10 | BP_7_10 | — | Kurtosis |
| 11 | Skewness | — | Skewness |
| 12 | BP_40_90 | — | — |

## ACKNOWLEDGMENTS

## AUTHOR DECLARATIONS

### Conflict of Interest

The authors have no conflicts to disclose.

### Author Contributions

**Lazar Tomcic:** Conceptualization (lead); Data curation (lead); Formal analysis (lead); Funding acquisition (supporting); Investigation (lead); Methodology (lead); Project administration (supporting); Resources (supporting); Software (lead); Supervision (supporting); Validation (lead); Visualization (lead); Writing – original draft (lead); Writing – review & editing (lead). **Armin Ederer:** Conceptualization (supporting); Data curation (supporting); Formal analysis (supporting); Investigation (supporting); Methodology (supporting); Software (supporting); Validation (supporting); Visualization (supporting); Writing – original draft (supporting); Writing – review & editing (supporting). **Sophie Grabmann:** Data curation (supporting); Investigation (supporting); Writing – original draft (supporting); Writing – review & editing (equal). **Michael Kick:** Conceptualization (supporting); Data curation (supporting); Writing – original draft (supporting); Writing – review & editing (equal). **Johannes Kriegler:** Conceptualization (supporting); Formal analysis (supporting); Visualization (supporting); Writing – original draft (supporting); Writing – review & editing (equal). **Michael F. Zaeh:** Funding acquisition (lead); Project administration (lead); Resources (lead); Supervision (lead); Writing – review & editing (equal).

## APPENDIX: PARAMETERS OF THE WELDING EXPERIMENTS PERFORMED

**TABLE III.** Parameters of the welding experiments performed.

**TABLE III.** (Continued.)

| No. | $P$ (W) | $v$ (mm/s) | No. | $P$ (W) | $v$ (mm/s) |
|---|---|---|---|---|---|
| 1 | 180 | 900 | 45 | 200 | 950 |
| 2 | 120 | 800 | 46 | 160 | 850 |
| 3 | 165 | 750 | 47 | 215 | 1000 |
| 4 | 140 | 900 | 48 | 225 | 900 |
| 5 | 200 | 850 | 49 | 280 | 1000 |
| 6 | 100 | 800 | 50 | 225 | 1000 |
| 7 | 110 | 1000 | 51 | 140 | 850 |
| 8 | 185 | 1000 | 52 | 345 | 1000 |
| 9 | 300 | 1000 | 53 | 320 | 1000 |
| 10 | 135 | 1000 | 54 | 100 | 900 |
| 11 | 115 | 1000 | 55 | 195 | 750 |
| 12 | 105 | 1000 | 56 | 175 | 800 |
| 13 | 290 | 1000 | 57 | 120 | 950 |
| 14 | 140 | 1000 | 58 | 185 | 750 |
| 15 | 150 | 800 | 59 | 135 | 750 |
| 16 | 180 | 800 | 60 | 150 | 1000 |
| 17 | 305 | 1000 | 61 | 270 | 1000 |
| 18 | 240 | 1000 | 62 | 330 | 1000 |
| 19 | 310 | 1000 | 63 | 175 | 1000 |
| 20 | 220 | 1000 | 64 | 335 | 1000 |
| 21 | 250 | 1000 | 65 | 220 | 900 |
| 22 | 190 | 1000 | 66 | 150 | 900 |
| 23 | 230 | 1000 | 67 | 110 | 950 |
| 24 | 130 | 1000 | 68 | 130 | 900 |
| 25 | 210 | 1000 | 69 | 190 | 900 |
| 26 | 180 | 1000 | 70 | 200 | 900 |
| 27 | 340 | 1000 | 71 | 110 | 850 |
| 28 | 380 | 1000 | 72 | 160 | 1000 |
| 29 | 350 | 1000 | 73 | 140 | 950 |
| 30 | 180 | 950 | 74 | 170 | 950 |
| 31 | 125 | 750 | 75 | 110 | 900 |
| 32 | 260 | 1000 | 76 | 100 | 1000 |
| 33 | 150 | 950 | 77 | 200 | 1000 |
| 34 | 100 | 850 | 78 | 110 | 800 |
| 35 | 170 | 800 | 79 | 230 | 900 |
| 36 | 140 | 800 | 80 | 120 | 1000 |
| 37 | 130 | 850 | 81 | 170 | 1000 |
| 38 | 160 | 800 | 82 | 120 | 900 |
| 39 | 105 | 750 | 83 | 145 | 1000 |
| 40 | 130 | 800 | 84 | 255 | 1000 |
| 41 | 170 | 900 | 85 | 160 | 900 |
| 42 | 210 | 900 | 86 | 265 | 1000 |
| 43 | 170 | 850 | 87 | 295 | 1000 |
| 44 | 155 | 750 | | | |

## REFERENCES

[1] Y.-L. Mao, G. Kinsman, and W. W. Duley, "Real-time fast Fourier transform analysis of acoustic emission during $CO_2$ laser welding of materials," J. Laser Appl. **5**, 17–22 (1993).

[2] H. Gu and W. W. Duley, "Analysis of acoustic signals detected from different locations during laser beam welding of steel sheet," in *Proceedings of International Congress on Laser Materials Processing, Laser Micro-Processing and Nanomanufacturing*, Detroit, MI, 14–17 October 1996 (Laser Institute of America, Orlando, FL, 1996), p. B40.

[3] D. F. Farson and K. R. Kim, "Generation of optical and acoustic emissions in laser weld plumes," J. Appl. Phys. **85**, 1329–1336 (1999).

[4] L. Li, "A comparative study of ultrasound emission characteristics in laser processing," Appl. Surf. Sci. **186**, 604–610 (2002).

[5] H. Gu and W. W. Duley, "A statistical approach to acoustic monitoring of laser welding," J. Phys. D: Appl. Phys. **29**, 556–560 (1996).

[6] W. Huang and R. Kovacevic, "Feasibility study of using acoustic signals for online monitoring of the depth of weld in the laser welding of

11 March 2025 13:05:28

high-strength steels," Proc. Inst. Mech. Eng. Part B: J. Eng. Manuf. **223**, 343–361 (2009).

[7]L. Schmidt, F. Römer, D. Böttger, F. Leinenbach, B. Straß, B. Wolter, K. Schricker, M. Seibold, J. Pierre Bergmann, and G. Del Galdo, "Acoustic process monitoring in laser beam welding," Proc. CIRP **94**, 763–768 (2020).

[8]K. Wasmer, T. Le-Quang, B. Meylan, F. Vakili-Farahani, M. P. Olbinado, A. Rack, and S. A. Shevchik, "Laser processing quality monitoring by combining acoustic emission and machine learning: A high-speed x-ray imaging approach," Proc. CIRP **74**, 654–658 (2018).

[9]S. A. Shevchik, T. Le-Quang, F. V. Farahani, N. Faivre, B. Meylan, S. Zanoli, and K. Wasmer, "Laser welding quality monitoring via graph support vector machine with data adaptive kernel," IEEE Access **7**, 93108–93122 (2019).

[10]M. F. M. Yusof, M. Ishak, and M. F. Ghazali, "Classification of weld penetration condition through synchrosqueezed-wavelet analysis of sound signal acquired from pulse mode laser welding process," J. Mater. Process. Technol. **279**, 116559 (2020).

[11]W. Huang and R. Kovacevic, "A neural network and multiple regression method for the characterization of the depth of weld penetration in laser welding based on acoustic signatures," J. Intell. Manuf. **22**, 131–143 (2011).

[12]M. F. M. Yusof, M. Ishak, and M. F. Ghazali, "Weld depth estimation during pulse mode laser welding process by the analysis of the acquired sound using feature extraction analysis and artificial neural network," J. Manuf. Process. **63**, 163–178 (2021).

[13]N. Authier, E. Touzet, F. Lücking, R. Sommerhuber, V. Bruyere, and P. Namy, "Coupled membrane free optical micro-phone and optical coherence tomography key-hole measurements to setup welding laser parameters," Proc. SPIE **11273**, 1127308 (2020).

[14]B. Fischer, "Optical microphone hears ultrasound," Nat. Photonics **10**, 356–358 (2016).

[15]H. E. Bass, L. C. Sutherland, and A. J. Zuckerwar, "Atmospheric absorption of sound: Update," J. Acoust. Soc. Am. **88**, 2019–2021 (1990).

[16]J. Sueur, T. Aubin, and C. Simonis, "Seewave: A free modular tool for sound analysis and synthesis," Bioacoustics **18**, 213–226 (2008).

[17]I. Guyon and A. Elisseeff, "An introduction to variable and feature selection," J. Machine Learning Res. **3**, 1157–1182 (2003).

[18]G. Sharma, K. Umapathy, and S. Krishnan, "Trends in audio signal feature extraction methods," Appl. Acoust. **158**, 107020 (2020).

[19]W. Huang and R. Kovacevic, "Acoustic monitoring of weld penetration during laser welding of high strength steels," in *Proceedings of the International Congress on Laser Materi-als Processing, Laser Microprocessing and Nanomanufacturing*, Orlando, FL, 2–5 November 2009 (Laser Institute of America, Orlando, FL, 2009), pp. 630–637.

[20]I. Daubechies, "The wavelet transform, time-frequency localization and signal analysis," IEEE Trans. Information Theory **36**, 961–1005 (1990).

[21]C. Torrence and G. P. Compo, "A practical guide to wavelet analysis," Bull. Am. Meteorol. Soc. **79**, 61–78 (1998).

[22]C. E. Rasmussen and C. K. I. Williams, *Gaussian Processes for Machine Learning* (MIT Press, Cambridge, MA, 2008).

[23]A. Karatzoglou, A. Smola, K. Hornik, and A. Zeileis, "Kernlab—An S4 package for kernel methods in R," J. Statistical Software **11**, 1–20 (2004).

[24]A. Vabalas, E. Gowen, E. Poliakoff, and A. J. Casson, "Machine learning algorithm validation with a limited sample size," PLoS ONE **14**, e0224365 (2019).

[25]I. Guyon, J. Weston, S. Barnhill, and V. Vapnik, "Gene selection for cancer classification using support vector machines," Mach. Learn. **46**, 389–422 (2002).

[26]J. Kroos, U. Gratzke, M. Vicanek, and G. Simon, "Dynamic behaviour of the keyhole in laser welding," J. Phys. D: Appl. Phys. **26**, 481–486 (1993).

[27]T. Klein, M. Vicanek, J. Kroos, I. Decker, and G. Simon, "Oscillations of the keyhole in penetration laser beam welding," J. Phys. D: Appl. Phys. **27**, 2023–2030 (1994).

[28]H. Gu and W. W. Duley, "Resonant acoustic emission during laser welding of metals," J. Phys. D: Appl. Phys. **29**, 550–555 (1996).

[29]L. Li and W. M. Steen, "Non-contact acoustic emission monitoring during laser processing," in *Proceedings of International Congress on Laser Materials Processing*, Orlando, FL, 25–29 October 1992 (Laser Institute of America, Orlando, FL, 1992), pp. 719–728.

[30]S. Ao, Z. Luo, M. Fend, and F. Yan, "Simulation and experimental analysis of acoustic signal characteristics in laser welding," Int. J. Adv. Manuf. Technol. **81**, 277–287 (2015).

[31]J. P. Campbell, "Speaker recognition: A tutorial," Proc. IEEE **85**, 1437–1462 (1997).

[32]C. H. Shadle, "Articulatory-acoustic relationships in fricative consonants," Speech Prod. Speech Modell. **55**, 187–209 (1990).

11 March 2025 13:05:28